Supplementary Information for: Optical spin locking of a solid-state qubit

J.H. Bodey,[1] R. Stockill,[1,*] E.V. Denning,[1,2] D.A. Gangloff,[1] G. Éthier-Majcher,[1]
D.M. Jackson,[1] E. Clarke,[3] M. Hugues,[4] C. Le Gall,[1,†] and M. Atatüre[1,‡]

[1] *Cavendish Laboratory, University of Cambridge, JJ Thomson Avenue, Cambridge, CB3 0HE, UK*
[2] *Department of Photonics Engineering, Technical University of Denmark, 2800 Kgs. Lyngby, Denmark*
[3] *EPSRC National Epitaxy Facility, University of Sheffield, Broad Lane, Sheffield, S3 7HQ, UK*
[4] *Université Côte d'Azur, CNRS, CRHEA, rue Bernard Gregory, 06560 Valbonne, France*

(Dated: September 10, 2019)

SUPPLEMENTARY NOTE 1: FURTHER NOTES ON THE EXPERIMENTAL SETUP

Figure S1 shows a schematic of the overall experimental setup. Three laser systems are combined and sent to the quantum dot (QD): a microwave-modulated Raman laser system (Toptica DL Pro, $\omega_R = 2\pi \times 309300$ GHz), a resonant laser to perform spin readout and initialisation (Newport NF laser, $\omega_1 = 2\pi \times 310051.2$ GHz), and a second resonant laser to perform repump during the nuclear-spin cooling process (MogLabs CatEye laser, $\omega_2 \approx \omega_1 + \delta$, where δ compensates for a $100 - 400$ -MHz shift in the transition frequency induced by the Raman laser). Both the laser excitation and fluorescence collection are achieved using a confocal microscope with an 0.5-NA objective lens. A cross-polarised detection minimises reflected resonant laser light, and a grating suppresses Raman laser light from the collection.

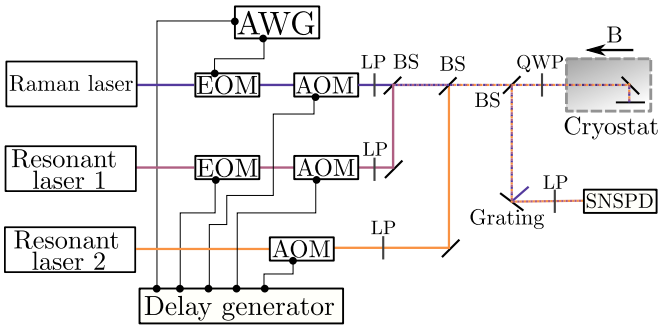

FIG. S1. A schematic of the experimental setup. Three continuous-wave lasers are passed through electro-optic modulators (EOMs) and acousto-optic modulators (AOMs) to build pulse sequences. The Raman-laser EOM is controlled by an arbitrary waveform generator (AWG). All other modulators are driven by delay generators, synchronised with the AWG. The lasers are combined using beamsplitters (BSs) and sent to a cryostat-housed QD device. Polarisation is controlled using a series of linear polarisers (LPs) and a quarter-wave plate (QWP), set such that the excitation is circularly polarised at the QD. Reflected laser light is minimised using a cross-polarised detection. A grating further suppresses the Raman laser background. The filtered collection is sent to a superconducting nanowire single-photon detector (SNSPD).

SUPPLEMENTARY NOTE 2: EFFECTIVE ESR FREQUENCY

A QD in Voigt geometry has two excited states ($|e\rangle$ and $|e'\rangle$, split by the hole Zeeman splitting ω_h), giving rise to two paths for the Raman process [1]. These paths interfere and the polarisation of the Raman beams, together with the phase-relationship between the optical transitions, dictates the effective ESR Rabi frequency. The Raman laser is circularly polarised thus driving each arm of the Λ-systems with equal strength following $\Omega = \Omega_L^2/(2\Delta_L)$ where Ω_L is the optical Rabi frequency and $\Delta_L = \Delta \pm \omega_h/2$ (Δ is defined in Figure 1 of the main text). The two Raman processes add up yielding an effective ESR frequency $\Omega = \Omega_L^2/\Delta$, in the limit $\omega_h \ll \Delta$.

SUPPLEMENTARY NOTE 3: RABI OSCILLATIONS

Decay of Rabi oscillations limited by spin decay

A resonantly driven 2-level system with a spin decay process (Γ_1) which depolarises the electron spin can be described by the master equation:

$$\dot{\rho} = -i[\Omega S_x, \rho] + \Gamma_1(L[S_-] + L[S_+])\rho, \tag{1}$$

where $S_x = \frac{1}{2}(|\uparrow\rangle\langle\downarrow| + |\downarrow\rangle\langle\uparrow|)$, $S_+ = |\uparrow\rangle\langle\downarrow|$, $S_- = |\downarrow\rangle\langle\uparrow|$ and $L(a)\rho = a\rho a^\dagger - \frac{1}{2}\{a^\dagger a, \rho\}$. The time evolution of the upper state population with the initial condition $\rho_{\uparrow\uparrow}(t = 0) = 1$ is:

$$\rho_{\uparrow\uparrow}(t) = \frac{1}{2}(1 + e^{-3/2\Gamma_1 t}[\cos\Big(\tilde{\Omega}t/2\Big) - \frac{\Gamma_1}{\tilde{\Omega}}\sin\Big(\tilde{\Omega}t/2\Big)]), \tag{2}$$

where $\tilde{\Omega} = \sqrt{4\Omega^2 - \Gamma_1^2}$. Spin Rabi at ESR frequencies $\Omega > 80$MHz has a coherence limited by the extrinsic laser-induced spin decay $\Gamma_1 \ll \Omega$, yielding a $1/e$-time $(3/2\Gamma_1)^{-1}$ and a Q factor $\approx \frac{4\Omega}{3\Gamma_1}$.

Extraction of the $1/e$ time, Q factor and pulse fidelity

We measure Rabi oscillations as presented in Figure S2, up to ESR pulse lengths of 790 ns. For each dataset

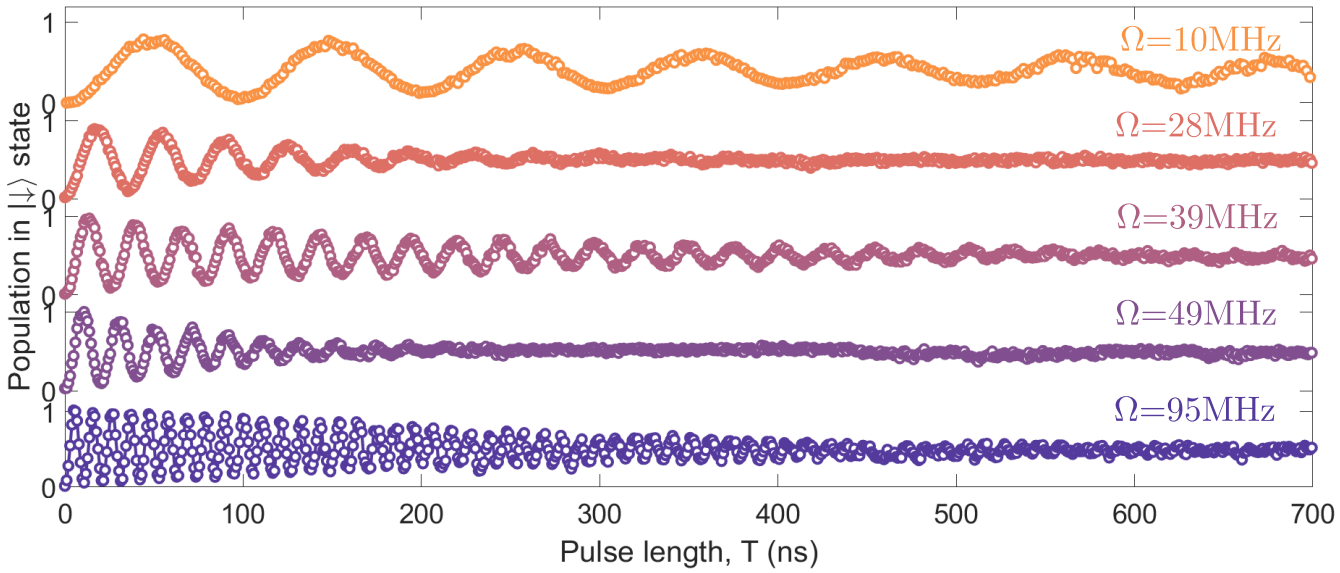

FIG. S2. Rabi oscillations at a set of different Rabi frequencies, illustrating the three regimes of (i) low Rabi frequency (10 MHz, top data), long decay time (ii) intermediate Rabi frequency (28, 49 MHz, 2nd and 4th data from top), very short decay time (iii) high Rabi frequency (95 MHz, bottom data), short decay time, as detailed in the main text. Data at 39 MHz (middle data) belong to a region in the nuclear spectral density where coupling is low. These data were used to extract the decay times presented in the main text, where we measure up to a maximum pulse length of 790 ns.

we evaluate the visibility over a π-period and measure the $1/e$ time, after which the visibility has decayed to $1/e$ of its initial value. The Q factor is the ratio between this $1/e$ time and the π pulse time [$t_\pi = 1/(2\Omega)$]. In the high-power regime ($\Omega \gg \omega^z_{\rm nuc}$), where the decay of the Rabi envelope is well-described by an exponential, the fidelity of a π pulse is closely related to the Q factor following $f_\pi = 1/2(1 + e^{-\frac{1}{Q}})$. In the low-power regime ($\Omega \ll \omega^z_{\rm nuc}$), the fidelity of a π pulse can be obtained from fitting the Rabi oscillation to a two-level Bloch-equation model where we carry an averaging over a Gaussian detuning distribution of variance $\sigma_{\rm OH} = 4.8$ MHz (Figure S3). This two-level Bloch-equation model which includes the Figure 2 mechanisms - (i) inhomogeneous broadening $\sigma = 4.8$ MHz and (iii) spin decay $\Gamma_1 = \alpha\|\Omega\|$ with $\alpha = 2.7 \times 10^{-2}$ - is used to fit the experimental spin trajectory away from Hartmann-Hahn resonances [Figures 1(b), 3(a), 4(a), 4(b)].

Laser-induced spin decay

At Rabi frequencies above $\sim$ 80 MHz (beyond the Hartmann-Hahn resonances), our decay envelope and corresponding gate fidelity become limited by laser-induced decay. At $\Delta = 700$ GHz, the decay is $\sim 10^2$ times faster than the photon scattering rate expected for ideal optical transitions (at our highest ESR drive $\Omega \sim 160$ MHz, the photon scattering rate is $2\Gamma_0\Omega_L^2/\Delta_L^2 \approx 60$ kHz, where $\Gamma_0 \sim 140$ MHz is the optical linewidth). The identification of a laser-induced

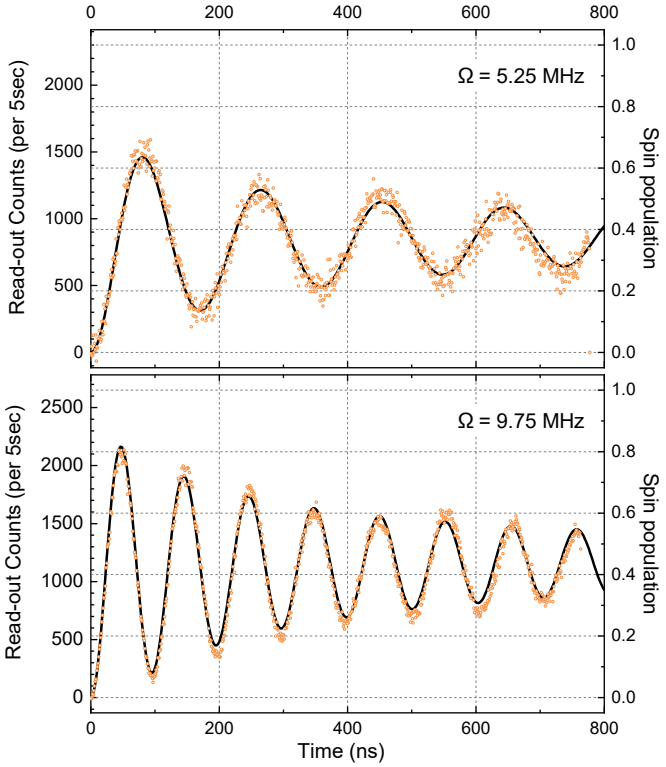

FIG. S3. Fidelity of ESR rotations at low Rabi frequencies. The spin population can be reconstructed from a two-level master equation model that accounts for nuclear-field inhomogeneities (black curve), yielding a π-pulse fidelity of $\sim 60\%$ at $\Omega \approx 5$ MHz and $\sim 80\%$ at $\Omega \approx 10$ MHz.

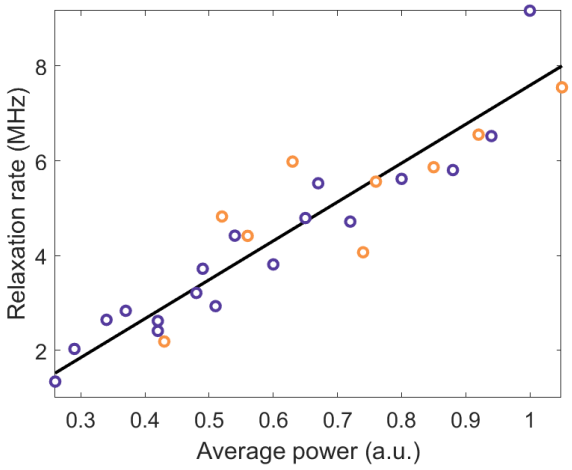

FIG. S4. Laser-induced spin relaxation as a function of input laser power, where the purple (yellow) circles indicate a laser detuning Δ of 800 GHz (1600 GHz). The black line is a linear fit to the data. The independence of relaxation rate from detuning indicates that this process is unrelated to the optical transitions of the QD.

spin decay is further supported by pump-probe measurements presented in Figure S4, where we measure the spin relaxation due to a detuned laser pulse (in the absence of any EOM modulation). The spin-relaxation rate increases linearly with the pulse power. If we increase the detuning (from 800 GHz to 1600 GHz) but keep the power constant, we observe the same decay rate.

In previous work, it was proposed that incoherent processes such as trion dephasing led to the creation of excited state population [1]. However, the optical decoherence that has to be included to model the Rabi decay in Figure 2 of the main text is incompatible with the close-to-lifetime-limited linewidth measured in resonance fluorescence. Phonons can also be ruled out both theoretically (we estimate phonon-absorption to be 10^2-times smaller than off-resonant photon-scattering) and by our decay measurement (the exponentially suppressed phonon absorption beyond $k_B T \approx 80$ GHz would lead to very different decays at 800 GHz and 1600 GHz which is not the case for the decay observed here). Lastly, in our device, this laser-induced decay is even more pronounced for hole spins ($f_\pi \approx 0.92$ with ultrafast rotations or ESR rotations). Our observation of a detuning-independent laser-induced decay and qubit-dependent fidelities points towards non-resonant processes occurring directly within the ground-state manifold.

SUPPLEMENTARY NOTE 4: INTERACTIONS WITH THE NUCLEAR-SPIN BATH

Non-Markovian master equation

The Hamiltonian describing the driven central electron and the nuclear-spin bath, after a Schrieffer-Wolff transformation that yields the effective low-energy dynamics in the presence of lattice strain, is [2, 3],

$$H = H_{\rm e} + H_{\rm n} + H_{\rm hf} + H_{\rm nc}, \tag{3}$$

where $H_{\rm e}$ describes the driven electron, $H_{\rm n} = \sum_j \omega^z_{\rm nuc} I^j_z + \Delta^j_Q (I^j_z)^2$ describes the free evolution of the nuclei, $H_{\rm hf} = \sum_j 2A^j I^j_z S_z$ is the low-energy part of the hyperfine interaction and $H_{\rm nc} = -S_z V_{\rm n}$, with

$$V_{\rm n} = \sum_j \frac{A^j B^j_Q}{\omega^z_{\rm nuc}} \times \{[(I^j_x)^2 - (I^j_y)^2]\cos^2\theta^j + [I^j_x I^j_z + I^j_z I^j_x]\sin 2\theta^j\} \tag{4}$$

describes a non-collinear strain-induced hyperfine interaction. Here, $\omega^z_{\rm nuc}$ is the nuclear Zeeman splitting, A^j, B^j_Q and $(\frac{\pi}{2} - \theta^j)$ are the hyperfine interaction strength, the quadrupolar coupling strength and the quadrupolar angle relative to the magnetic field for the j'th nucleus, and $\Delta^j_Q = B^j_Q(\sin^2\theta^j - \frac{1}{2}\cos^2\theta^j)$ is the associated quadrupolar energy shift. The Overhauser field, $\Delta = \sum_j 2A^j I^j_z$ is modelled as a quasi-static classical variable [4] and is absorbed into $H_{\rm e} = \Omega S_x + \Delta S_z$. This non-interacting electron Hamiltonian can be diagonalised under the unitary transformation $H \to \tilde{H} = e^{i\phi S_y} H e^{-i\phi S_y}$, where $\sin\phi = \Omega/\Omega'$, $\cos\phi = \Delta/\Omega'$ and $\Omega' = \sqrt{\Omega^2 + \Delta^2}$. The transformed terms in the Hamiltonian are then $\tilde{H}_{\rm e} = \Omega' S_z$, $\tilde{H}_{\rm n} = H_{\rm n}$, $\tilde{H}_{\rm nc} = (S_x \sin\phi - S_z \cos\phi)V_{\rm n}$.

To obtain the reduced dynamics of the electron spin density operator, ρ, we derive a quantum master equation, where the nuclear bath is traced out. When the system is operated in the vicinity of the Hartmann-Hahn resonance, the most significant contribution to the dynamics is expected to arise from the secular electron–nuclear transitions generated by $\tilde{H}_{\rm nc}$. Therefore, to simplify the analysis, we start out by removing the non-secular terms therein, obtaining $\tilde{H} \to \frac{1}{2}\sin\phi(S_- V^+_{\rm n} + S_+ V^-_{\rm n})$, where

$$V^+_{\rm n} = \frac{1}{2}\sum_j A^j_{\rm nc}\Big[(I^j_+)^2\cos^2\theta_j + (I^j_+ I^j_z + I^j_z I^j_+)\sin 2\theta^j\Big], \tag{5}$$

$A^j_{\rm nc} = \frac{A^j B^j_Q}{\omega^z_{\rm nuc}}$, $V^-_{\rm n} = (V^+_{\rm n})^\dagger$ and $S_\pm = S_x \pm iS_y$, $I^j_\pm = I^j_x \pm iI^j_y$ are the electron- and nuclear-spin transition operators. The corresponding non-Markovian time-

convolutionless master equation for ρ is [5]

$$\frac{\partial}{\partial t}\rho = -i[\Omega' S_z, \rho] - \int_0^t \mathrm{d}\tau\, \mathrm{Tr}_\mathrm{n}[\tilde{H}_\mathrm{nc}, [\tilde{H}_\mathrm{nc}(-\tau), \rho \otimes \rho_\mathrm{n}^0]] \tag{6}$$

where $\tilde{H}_\mathrm{nc}(-\tau) = e^{-i(\tilde{H}_\mathrm{e}+\tilde{H}_\mathrm{n})\tau}\tilde{H}_\mathrm{nc}e^{+i(\tilde{H}_\mathrm{e}+\tilde{H}_\mathrm{n})\tau}$ denotes the interaction picture time evolution of $\tilde{H}_\mathrm{nc}$ and ρ_n^0 is the reference state of the nuclear bath. Following Ref. [6], we assume that the nuclear reference state is factorisable among the nuclei. Furthermore, we assume that the relevant features contributing to the non-collinear processes in the master equation, Eq. (6), can be described by a thermal nuclear density operator at infinite temperature. Under these assumptions, we arrive at the following master equation for the electron spin,

$$\frac{\partial}{\partial t}\rho(t) = -i[\Omega' S_z, \rho(t)] + \Gamma(\Omega', t)(L(S_+) + L(S_-))\rho(t), \tag{7}$$

where the nuclear-induced Lamb shift has been neglected, $L(x)\rho = x^\dagger \rho x - \frac{1}{2}\{xx^\dagger, \rho\}$ is the Lindblad dissipator and

$$\Gamma(\Omega', t) = \frac{\sin^2\phi}{4}\frac{1}{\pi}\int \mathrm{d}\omega\, \mathcal{D}(\omega)\frac{\sin[(\omega-\Omega')t]}{\omega-\Omega'} \tag{8}$$

is a time-dependent decay rate calculated from the spectral density, $\mathcal{D}(\omega) = \mathcal{D}^{(1)}(\omega) + \mathcal{D}^{(2)}(\omega)$, which contains contributions from the nuclear processes changing the total nuclear polarisation by one or two units,

$$\begin{aligned}\mathcal{D}_1(\omega) = &\frac{\pi}{2}\sum_j \frac{(A_\mathrm{nc}^j \sin 2\theta^j)^2}{2I^j+1} \\ &\sum_{m_j=-I^j}^{I^j-1}[M_+(I^j, m_j)(2m_j+1)]^2 \\ &\times \delta(\omega - [\omega_\mathrm{nuc}^z + (2m_j+1)\Delta_Q^j]),\end{aligned} \tag{9}$$

$$\begin{aligned}\mathcal{D}_2(\omega) = &\frac{\pi}{2}\sum_j \frac{(A_\mathrm{nc}^j \cos^2\theta^j)^2}{2I^j+1} \\ &\sum_{m_j=-I^j}^{I^j-2}[M_+(I^j, m_j)M_+(I^j, m_j+1)]^2 \\ &\times \delta(\omega - [2\omega_\mathrm{nuc}^z + 4\Delta_Q^j(m_j+1)]),\end{aligned}$$

where $M_+(I,m) = \sqrt{I(I+1)-m(m+1)}$ and I^j is the total spin eigenvalue for the j'th nucleus. The next step is to split the summation over nuclei into a summation over nuclear species, s, such that $\mathcal{D}^{(i)} = \sum_s \mathcal{D}_s^{(i)}$. For each species, the total nuclear spin is constant, $I^j = I_s$, and the parameters $(\theta, B_Q, A) =: \xi$ are described by a statistical distribution over the nuclear ensemble, $P_s(\xi)$, for the given species, s. We then approximate the summation over nuclei in Eq. (9) as an integral over this distribution, $\sum_j f_s^j \simeq N_s \int \mathrm{d}\xi\, P_s(\xi) f_s(\xi)$, where N_s is the number of nuclei of species s and f_s^j is a general function of single-nucleus parameters of that species. Taking the distribution $P(\xi)$ to be factorisable, $P_s(\xi) = p_{s,1}(\theta)p_{s,2}(B_Q)p_{s,3}(A)$, we find

$$\begin{aligned}\mathcal{D}_s^{(1)}(\omega) = &\frac{\pi}{2}\frac{\langle A^2\rangle_s N_s}{2I_s+1}\sum_{m=-I_s}^{I_s-1}[M_+(I_s,m)(2m+1)]^2 \\ &\times \int \mathrm{d}\theta\, p_1(\theta)p_2\left[\frac{\omega-\omega_\mathrm{nuc}^z}{(2m+1)(\sin^2\theta - \frac{1}{2}\cos^2\theta)}\right] \\ &\times \left(\frac{(\omega-\omega_\mathrm{nuc}^z)\sin 2\theta}{\omega_\mathrm{nuc}^z(2m+1)(\sin^2\theta-\frac{1}{2}\cos^2\theta)}\right)^2 \\ &\times \left|(2m+1)\left(\sin^2\theta - \frac{1}{2}\cos^2\theta\right)\right|^{-1} \\ \mathcal{D}_s^{(2)}(\omega) = &\frac{\pi}{4}\frac{\langle A^2\rangle_s N_s}{2I_s+1}\sum_{m=-I_s}^{I_s-2}[M_+(I_s,m)M_+(I_s,m+1)]^2 \\ &\times \int \mathrm{d}\theta\, p_1(\theta)p_2\left[\frac{\omega-2\omega_\mathrm{nuc}^z}{4(m+1)(\sin^2\theta - \frac{1}{2}\cos^2\theta)}\right] \\ &\times \left(\frac{(\omega-2\omega_\mathrm{nuc}^z)\cos^2\theta}{4\omega_\mathrm{nuc}^z(m+1)(\sin^2\theta-\frac{1}{2}\cos^2\theta)}\right)^2 \\ &\times \left|2(m+1)\left(\sin^2\theta - \frac{1}{2}\cos^2\theta\right)\right|^{-1},\end{aligned} \tag{10}$$

where $\langle A^2\rangle_s = \int \mathrm{d}A\, p_{s,3}(A)A^2$.

Transforming back to the Zeeman eigenbasis, the master equation is

$$\begin{aligned}\frac{\partial}{\partial t}\rho(t) = &-i[\Delta S_z + \Omega S_x, \rho(t)] \\ &+ \Gamma(\Omega', t)\{L(S_\phi) + L(S_\phi^\dagger)\}\rho(t),\end{aligned} \tag{11}$$

where $S_\phi = S_x\cos\phi + iS_y + S_z\sin\phi$. Finally, we add the terms $\Gamma_1(L(S_+) + L(S_-))\rho(t)$ and $\Gamma_2 L(S_z)$ to the master equation, where Γ_1 is the extrinsic laser-induced spin-decay process and Γ_2 is the spin coherence decay measured in Hahn-Echo, $1/(2.8\ \mu\mathrm{s})$.

Parameter probability distributions

The probability distributions for the hyperfine and quadrupolar coupling strengths, $p_{s,2}$ and $p_{s,3}$ are taken Gaussian. The major quadrupolar axis distribution is assumed to be symmetric around the QD growth axis, characterised by a uniform distribution of the azimuthal angle, φ' and a Gaussian distribution for the polar angle, θ'. The equivalent distribution for the θ-angle appearing in Eq. (4) is obtained by rotating the coordinate system around the magnetic field axis (the x-axis), such that the quadrupolar angle is lying in the xz-plane. Denoting the

	Indium	Arsenic
B_Q (MHz)	1.29	3.7
σ_{B_Q} (MHz)	0.45	1.5
θ' (degrees)	17	15.2
$\sigma_{\theta'}$ (degrees)	12	10
A (GHz/N_{tot})	26.6/N_{tot}	20.8/N_{tot}
σ_A (GHz/N_{tot})	26.6/N_{tot}	20.8/N_{tot}
N	18500	37000

TABLE S1. Summary of the nuclear parameters taken in our model. To reduce the number of free parameters in our model, we assume a QD composition of $In_{0.5}Ga_{0.5}As$, and set the standard deviation of strain parameters to values used previously in [7]. The parameters which are fitted to the Hartmann-Hahn spectrum of this QD is the total number of nuclei ($N_{tot} = 74000$), the quadrupolar field B_Q and quadrupolar angle θ for Indium and Arsenic. The contribution of Gallium is neglected as its nuclear spectral density is much smaller than that of Arsenic and Indium [7].

Gaussian polar probability distribution for the nuclear species s by $p_{s,\mathrm{p}}(\theta')$, the distribution for θ is found to be

$$p_{s,1}(\theta) = \frac{1}{\pi}\int_{\theta}^{\pi-\theta} \mathrm{d}\theta' \, \frac{p_{s,\mathrm{p}}(\theta')\cos(\theta)\sin\theta'}{\sqrt{\sin^2\theta' - \sin^2\theta}}, \tag{12}$$

where θ is defined to be in the range $[0, \pi]$.

Rabi decay rate

Due to the non-Markovianity of the electron-spin time evolution, a decay rate of the Rabi oscillations is in principle not well-defined. However, the non-Markovian effects are most strongly pronounced at short times, whereas in the long-time limit, the system approaches the Markovian limit. Effectively, the electron spin probes the spectral density at the Rabi frequency during a finite time window corresponding to the decay time. This can be encoded into the calculation of the dynamics by employing a self-consistent Born-Markov approximation [8, 9]. Here, we implement such an approach by first writing the Markov limit for the nuclear transition induced electron decay rate,

$$\Gamma_{\mathrm{M}}(\Omega') = \frac{1}{4}\sin^2\phi\,\mathrm{Re}\left[\int_0^\infty \mathrm{d}\tau\, e^{-i\Omega'\tau}\int_{-\infty}^{\infty}\frac{\mathrm{d}\omega}{2\pi}\mathcal{D}(\omega)e^{i\omega\tau}\right]. \tag{13}$$

Here, the exponential factor $e^{-i\Omega'\tau}$ appears through the free evolution of the electronic $S_\pm$ operators. In our self-consistent Born-Markov approach, we encode the decay of the electron spin into this correlation function, replacing it by $e^{-[i\Omega'+\gamma(\Omega')]t}$. The damping rate, $\gamma(\Omega')$, is then determined self-consistently through an iterative process. By replacing the free correlation function by the damped one, we define a self-consistent Markovian decay rate,

$$\begin{aligned}\Gamma_{\mathrm{SCM}}(\Omega') &= \frac{\sin^2\phi}{4}\times 2\,\mathrm{Re}\Big[\int_0^\infty \mathrm{d}\tau\, e^{-[i\Omega'+\gamma(\Omega')]\tau} \\ &\qquad\times\int_{-\infty}^{\infty}\frac{\mathrm{d}\omega}{2\pi}\mathcal{D}(\omega)e^{i\omega\tau}\Big] \\ &= \frac{\sin^2\phi}{4}\int_{-\infty}^{\infty}\mathrm{d}\omega\,\mathcal{D}(\omega)\frac{1}{\pi}\frac{\gamma(\Omega')}{\gamma(\Omega')^2+(\omega-\Omega')^2},\end{aligned} \tag{14}$$

which describes a convolution of the spectral density with a Lorentzian distribution. Furthermore, we also average over the configurations of the Overhauser field, which is taken as a Gaussian distribution with standard deviation σ_{OH}, leading to the averaged decay rate

$$\begin{aligned}\tilde{\Gamma}_{\mathrm{SCM}}(\Omega) &= \frac{1}{4}\int\mathrm{d}\Delta\int_{-\infty}^{\infty}\mathrm{d}\omega\,\frac{\Omega^2}{\Delta^2+\Omega^2}\mathcal{D}(\omega) \\ &\qquad\times\frac{e^{-\Delta^2/2\sigma_{\mathrm{OH}}^2}}{\sqrt{2\pi\sigma_{\mathrm{OH}}^2}}\frac{1}{\pi}\frac{\gamma(\Omega')}{\gamma(\Omega')^2+(\omega-\Omega')^2}.\end{aligned} \tag{15}$$

To self-consistently determine $\tilde{\Gamma}_{\mathrm{SCM}}(\Omega)$ and $\gamma(\Omega')$, we start out by letting $\gamma(\Omega') = \frac{1}{4}\mathcal{D}(\Omega) + \frac{3}{2}\Gamma_1 + \Gamma_2$ and calculate the first iteration of the decay rate, $\tilde{\Gamma}^{(1)}_{\mathrm{SCM}}(\Omega)$. In the next iteration, we set $\gamma(\Omega') = \tilde{\Gamma}^{(1)}_{\mathrm{SCM}}(\Omega) + \frac{3}{2}\Gamma_1 + \Gamma_2$ and repeat this procedure until the iterative series has converged.

* Present address: Kavli Institute of Nanoscience, Delft University of Technology, Lorentzweg 1, 2628 CJ Delft, The Netherlands
† Electronic address:cl538@cam.ac.uk
‡ Electronic address: ma424@cam.ac.uk

[1] Press, D., Ladd, T. D., Zhang, B. & Yamamoto, Y. Complete quantum control of a single quantum dot spin using ultrafast optical pulses. *Nature* **456**, 218–221 (2008).
[2] Denning, E. V., Gangloff, D. A., Atatüre, M., Mørk, J. & Le Gall, C. Collective quantum memory activated by a driven central spin (2019). arXiv:1904.11180.
[3] Gangloff, D. *et al.* Quantum Interface of an Electron and a Nuclear Ensemble. *Science* **364**, 62–66 (2018).
[4] Merkulov, I. A., Efros, A. L. & Rosen, M. Electron spin relaxation by nuclei in semiconductor quantum dots. *Physical Review B* **65**, 205309 (2002).
[5] Breuer, H.-P. & Petruccione, F. *The Theory of Open Quantum Systems* (Oxford University Press, 2007).
[6] Coish, W. A., Fischer, J. & Loss, D. Free-induction decay and envelope modulations in a narrowed nuclear spin bath. *Physical Review B* **81**, 165315 (2010).
[7] Stockill, R. *et al.* Quantum dot spin coherence governed by a strained nuclear environment. *Nature Communications* **7**, 12745 (2016).
[8] Esposito, M. & Galperin, M. Self-consistent quantum master equation approach to molecular transpor. *Journal of Physical Chemistry C* **114**, 20362–20369 (2010).

[9] Jin, J., Li, J., Liu, Y., Li, X. Q. & Yan, Y. Improved master equation approach to quantum transport: From Born to self-consistent Born approximation. *Journal of Chemical Physics* **140**, 244111 (2014).